THE MECHANICS OF MOTILITY IN DISSOCIATED CYTOPLASM

MICAH DEMBO
Theoretical Biophysics, Theoretical Division, Los Alamos National Laboratory, Group T-10, Mail Stop K710, Los Alamos, New Mexico 87545

ABSTRACT We stimulate the dynamical behavior of dissociated cytoplasm using the Reactive Flow Model (Dembo, M., and F. Harlow, 1986, *Biophys. J.*, 50:109–121). We find that for the most part the predicted dynamical behavior of the cytoplasm is governed by three nondimensional numbers. Several other nondimensional parameters, the initial conditions, and boundary conditions are found to have lesser effects. Of the three major nondimensional parameters, one ($D^\sharp$) controls the percentage of ectoplasm, the second ($C^\sharp$) controls the sharpness of the endoplasm–ectoplasm boundary, and the third ($R^\sharp$) controls the topological complexity of the endoplasm–ectoplasm distribution.

If $R^\sharp$ is very small, then the cytoplasm contracts into a single uniform mass, and there is no bulk streaming. If $R^\sharp$ is very large, then the cytoplasmic mass breaks up into a number of clumps scattered throughout the available volume. Between these clumps the solution undergoes turbulent or chaotic patterns of streaming. Intermediate values of $R^\sharp$ can be found such that the mass of cytoplasm remains connected and yet undergoes coherent modes of motility similar to flares (Taylor, D.L., J.S. Condeelis, P.L. Moore, and R.D. Allen, 1973, *J. Cell Biol.*, 59:378–394) and rosettes (Kuroda, K., 1979, Cell Motility: Molecules and Organization, 347–362).

INTRODUCTION

The reactive flow model is a putative description of motile cytoplasm based on the formalism of multifield fluid mechanics (Dembo and Harlow, 1986). In this model the cytoplasm is viewed as a finely divided mixture of two distinct material phases: an isotropic contractile network of actin and myosin filaments and an aqueous solution. The laws of mass and momentum conservation for such a system, as well as the incompressibility condition, are formulated in terms of a system of field equations.

In the reactive flow model we usually assume that the cytoplasm is enclosed within a fixed region of space called a "reaction vessel." Much of the physical content of the model is expressed by the detailed boundary conditions used to describe the many possible interactions that can occur between the network and solution phases and the surrounding material.

For easy reference the field equations of the reactive flow model, as well as boundary conditions of relevance to the present discussion, are summarized in Appendix A. The various symbols we use to denote important coefficients and variables of the model are listed and defined in Table I.

A numerical algorithm for solving the reactive flow model has been developed for the special case of a two-dimensional reaction vessel with rectangular boundaries (Dembo et al., 1986). This algorithm has been applied for the analysis of some simple experimental systems involving so-called unreactive or slowly reactive contractile networks (Dembo et al., 1986). Here we will consider two experimental systems in which chemical reaction is an essential part of the dynamics. One system under study will be the dissociated cytoplasm of the giant carnivorous ameba, *Chaos carolinensis* (Taylor et al., 1973). We will also consider the behavior of cytoplasm removed from the acellular slime mold, *Physarum polycephalum* (Kuroda, 1979).

EXPERIMENTAL BACKGROUND

The first description of motility in dissociated cytoplasm seems to be due to Allen et al. (1960). These authors reported that dissociated cytoplasm of a single organism of the species *Chaos chaos* would continue active motility for several minutes when confined to a narrow glass capillary tube. Immediately after the rupture of the cell membrane, the cytoplasm flowed in the fountain pattern typical of the intact organism. However, this pattern was not stable and rapidly devolved into a state of random or chaotic streaming. Random or chaotic streaming was also reported by Thompson and Wolpert (1963) and by Pollard and Ito (1970) using pooled high-speed extracts of cytoplasm from *Amoeba proteus*.

In their study of *Chaos* cytoplasm, Taylor et al. (1973) observed several distinct modes of behavior, depending on the composition of the physiological medium. The so-called stabilized state of the cytoplasm occurred if the cell membrane of a single ameba was ruptured after the organism has been placed in a physiological medium lacking both ATP and free calcium ion. In this medium the cytoplasm flowing from the ruptured membrane rapidly lost its fluidity and turned into an inert viscoelastic mass that adhered to glass surfaces. The solidified cytoplasm was quite stable for long periods and could be separated easily from the remnants of the cell membrane. The stabilized state was viewed as analogous to the state of rigor in muscle.

If the stabilization medium was replaced by medium lacking calcium

TABLE I
PHYSICAL PARAMETERS OF THE REACTION FLOW MODEL

Dependent variables	
$\theta_s(x, y, t)$	Solution volume fraction
$\theta_n(x, y, t)$	Network volume fraction
$\Omega_n(x, y, t)$	Network velocity field
$\Omega_s(x, y, t)$	Solution velocity field
$P_F(x, y, t)$	Effective pressure field
R_{CD}	Threshold value of rending number for C → D transition
R_{DE}	Threshold value of rending number for D → E transition
$\hat{\theta}_n$	Network volume fraction at mechanical equilibrium
Independent variables	
$\tilde{\theta}_n$	Network volume fraction at chemical equilibrium
T_{eq}	Chemical relaxation time of network synthesis and breakdown
σ	Swelling number
Ψ_F	Effective contractile stress
Φ	Drag coefficient
M_n	Network shear viscosity
Λ_n	Network dilation viscosity
M_s	Solution shear viscosity
Λ_s	Solution dilation viscosity
L_x and L_y	X and Y dimensions of reaction vessel

ion but containing ~1 mM Mg^{+2}-ATP (relaxation medium), then the cytoplasm remained passive but gradually regained its fluidity. In this condition the cytoplasm was said to be in the relaxed state. Transient contraction to a small percentage of initial volume was observed if the relaxation medium was supplemented by adding calcium ion in excess of 1 μm (contraction medium).

To obtain a state of continuing automatic motion, Taylor et al. (1973) used a medium containing Mg^{+2}-ATP together with a level of free calcium ion just above the threshold required for contraction (i.e., $\sim 0.7 \times 10^{-6}$ M). The form of motility produced under these conditions typically consisted of numerous fountains or loops of flowing material. The fountains erupted from the cytoplasmic mass at various points, flowed outwards for up to several hundred microns, and then return toward the central mass. (A micrograph of a cytoplasmic mass undergoing this form of motility is shown in Fig. 1.) The streaming fountains of cytoplasm were called "flares" because of their resemblance to solar prominences. The medium containing threshold calcium together with Mg^{+2}-ATP was called flare solution.

In the studies of Taylor et al. (1973), the duration of the flaring reaction was usually between 10 and 20 min. Taylor et al. did not describe the detailed properties of their system after flaring activity had subsided. During the flaring reaction the maximum velocity of flow in the outward streaming arm of a flare was typically in the range of 20–50 μm/s. The returning arm of a typical flare flowed at a much slower rate, and in some cases the returning arm did not flow at all (range 0–12 μm/s). In addition to its greatly reduced flow rate, the material in the returning arm of a cytoplasmic flare had a much higher refractive index than the material in the outward flowing arm. This change in refractive index occurred near the outermost extremity of the flare and was presumed to represent a change in the density of contractile filaments.

The change in refractive index at the tip of flares seems to be analogous to the endoplasmic–ectoplasmic transition that occurs near the tip of intact pseudopods of *Chaos carolinensis*. The size of flares, the speed of outward flow, and the slower speed of return flow are also typical of the so-called fountain flow observed in intact pseudopods.

Kuroda (1979) has reported observations of cytoplasm from *Physarum polycephalum* that differ in some details from the observations of *Chaos* cytoplasm. In the case of *Physarum*, cytoplasm was obtained by extruding a drop of endoplasm after puncture of the plasmodium. The cytoplasm thus obtained was quickly transferred to a special solution that inhibited remembranation. The central cytoplasmic mass had a diameter of up to 1,000 μm and exhibited many fountains of flowing material up to 300-μm long. Vigorous fountain flow continued for 30 min or longer (see Fig. 1 *B*). The convection cells were tightly packed and completely covered the surface of the cytoplasmic mass, giving rise to a so-called "rosette" morphology. The flow velocity in the individual fountains was up to 100 μm/s at the point of eruption (the velocity of return flow was not reported). No difference in refractive index could be observed between the outgoing and returning streams. Nevertheless, filaments could be seen to form and contract at the extremities of individual flares. Kuroda did not describe the effects of changing the physiological medium; in particular, an analogue of the relaxed state was not described.

After ~30 min of continuous fountain activity, Kuroda observed that the cytoplasmic mass appeared to lose its coherence and began to slowly "spread out." Within this more diffuse organization of filaments, Kuroda observed small foci of intense contractile activity called "contractile centers." Formation and contraction of filaments in the vicinity of the randomly scattered contractile centers continued for an additional 30 min. After this period, movement slowed and eventually stopped.

In summary, demembranated cytoplasm can exist in a stabilized state, a relaxed state, and can also exhibit states of continuing automatic motion. In many experiments the observed motility has been chaotic; however, two related forms of coherent motility (i.e., flaring and rosetting) have also been reported.

COMPUTATIONAL PROCEDURES

The Reaction Vessel

The existing algorithm for integrating the reactive flow model can only deal with a finite two-dimensional computational region that has fixed rectangular boundaries. With these limitations in mind, we must devise a reaction vessel that can in some sense contain or capture the dynamics of demembranated cytoplasm.

Fig. 2 shows a schematic of a cross-section through a cytoplasmic mass. We assume that motion does not occur perpendicular to the plane of section. Superimposed on the drawing in Fig. 2 are lines indicating boundaries or walls with which we propose to delimit a finite computational region. As shown, the computational region is rectangular with horizontal sides of length L_x and vertical sides of length L_y.

At the bottom wall of the reaction vessel we desire to represent the behavior of stagnant material deep within the cytoplasmic mass. At the top wall we desire to represent the behavior of material located beyond the outermost extent of mixing and disturbance at the surface of the mass. The left and right boundaries are simply artificial cutoff sections perpendicular to the surface of the cytoplasmic mass.

We have experimented with two approaches for dealing with the artificial left and right walls: periodic boundary conditions and mirror symmetry boundary conditions. Periodic boundary conditions were prone to induce certain artificial modes corresponding to rotations of the cytoplasmic mass about a central axis. We will therefore restrict consideration in our subsequent discussion to mirror symmetry conditions only.

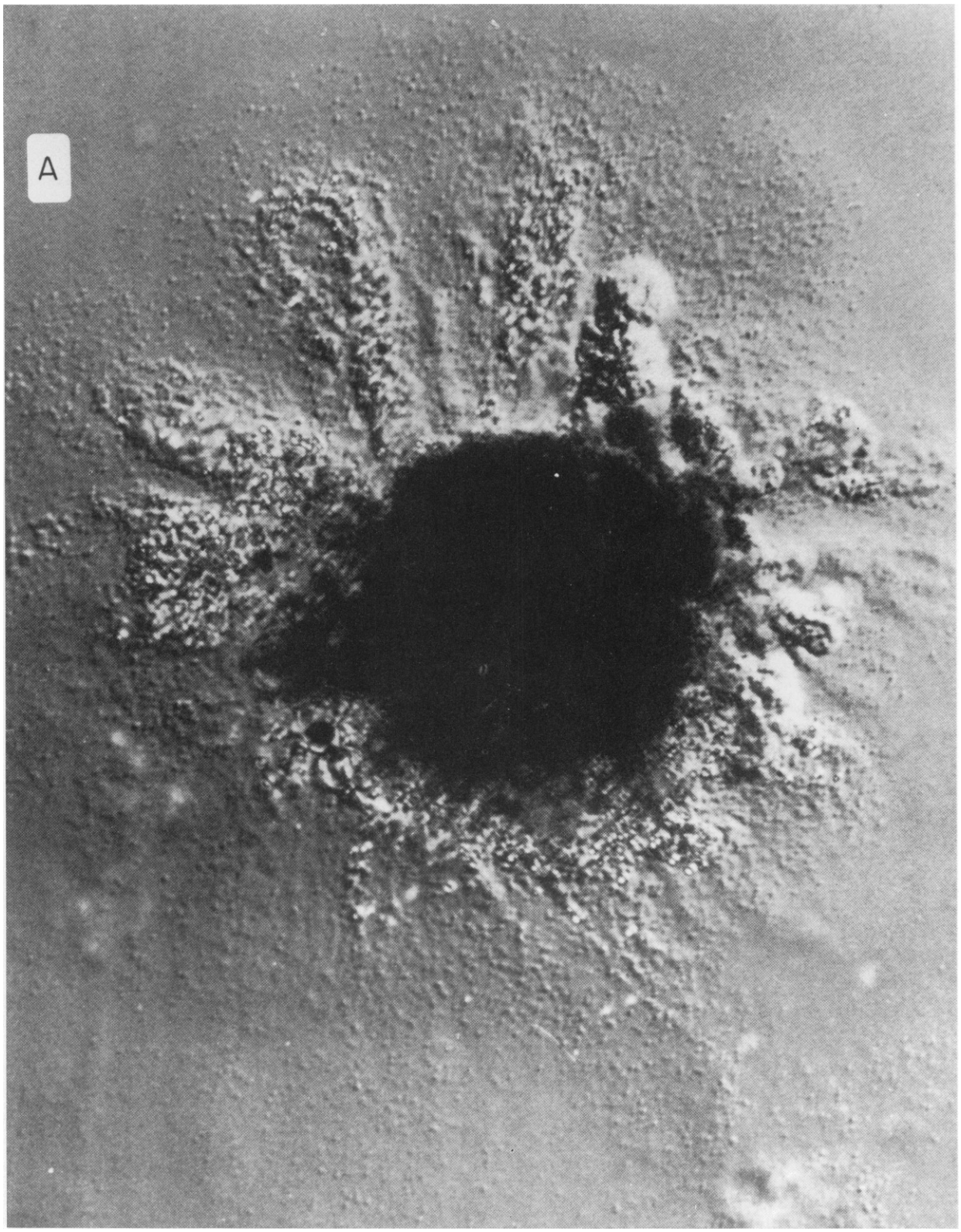

FIGURE 1 Experimental observations. (*A*) Dissociated cytoplasm of a single organism of the giant amoeba, *Chaos carolinensis*. Loops of streaming material (flares) extend out from the cytoplasmic mass. Field width equals 850 μm. Reproduced from Taylor et al. (1973) by copyright permission of the authors and Rockefeller University Press. (*B*) Demembranated droplet of cytoplasm removed from the plasmodium of *Physarum polycephalum*. Numerous lobes of streaming material completely surround the cytoplasmic mass forming a rosette morphology. Field width equals 2,000 μm. Reproduced from Kuroda (1979) by copyright permission of the author and the Yamada Science Foundation.

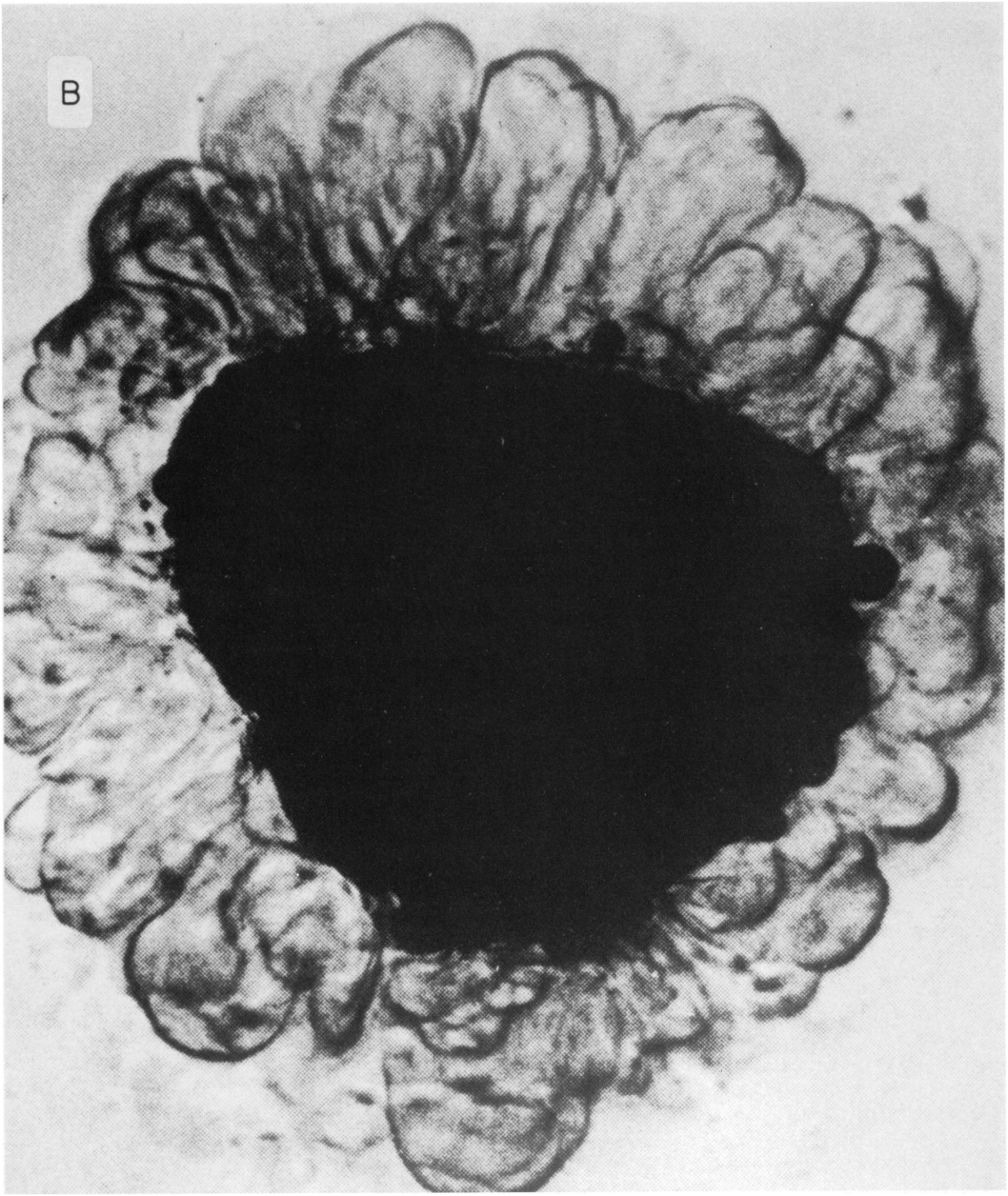

FIGURE 1B (*Continued*)

The condition of stagnation deep within the cytoplasmic mass is expressed by the vanishing of all components of velocity for both network and solution at the lower boundary. This treatment of the lower boundary seems plausible, but only under the assumption that the cytoplasmic mass is sufficiently large and stable. In particular, we expect difficulties if the cytoplasm tends to break up or "dissolve" in some manner (cf. Results). As a check on the assumption of stagnation of the solution phase, we have considered the effects of allowing positive hydraulic conductivity of the lower boundary (cf. Results).

We used two alternative methods of dealing with the

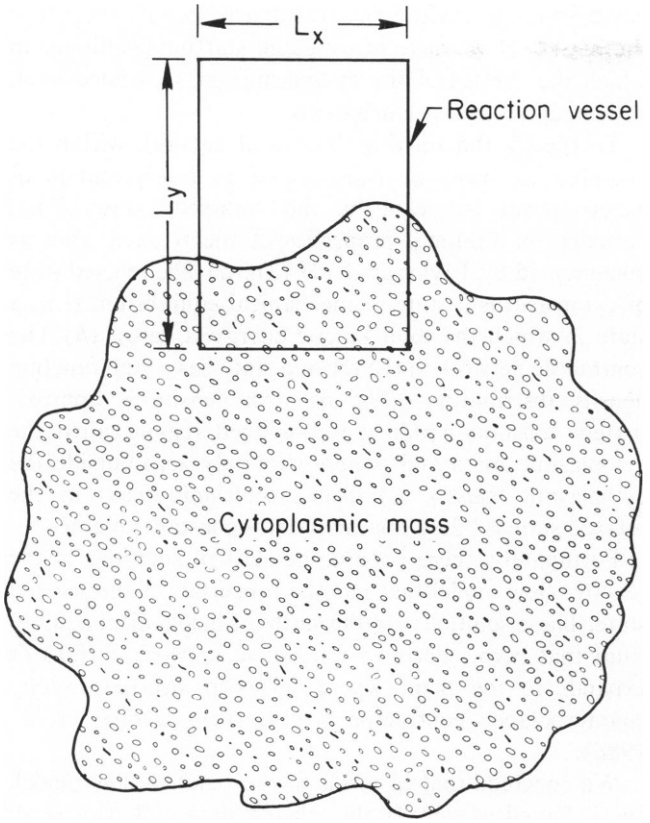

FIGURE 2 The reaction vessel. To capture the essential behavior of a dissociated mass of cytoplasm, we define an imaginary reaction vessel as shown. At the lower wall of the reaction vessel we employ boundary conditions that model the behavior of stagnant material well beneath the surface of the cytoplasmic mass. We attempt to place the upper wall at a position far enough above the surface of the mass so as to be outside the domain of dynamical interest. The left and right walls are regarded as simple mirror symmetry slip-planes.

boundary conditions at the top wall of the reaction vessel: the reservoir method and the no-stick method. In the no-stick method we assume that the top boundary is an impermeable barrier that is free-slip and that has no adhesive sites for network (e.g., an interface with air). An important aspect of this treatment is that, although the top boundary prevents upward flux of network, it offers no resistance if network material attempts to move in the downward direction. The detailed mathematical formulation of the no-stick boundary condition was discussed previously (Dembo and Harlow, 1986).

In the reservoir method we assume that the upper boundary represents a permeable interface between the reaction vessel and an infinite domain of homogeneous solution material at constant pressure.[1] This implies that the normal gradients of all components of velocity vanish outside the upper boundary. The main advantage of the reservoir method is that we do not prevent either network or solution material from passing out of the reaction vessel across the upper boundary. This much is quite realistic; however, unlike the real situation, network material that leaves the computational mesh is assumed to be instantly annihilated due to depolymerization or mixing with an infinite amount of solution material. Furthermore, we assume that de novo chemical formation of network in the reservoir is negligible. Thus, the only phase that is allowed to re-enter the reaction vessel from the reservoir is the solution phase.

[1]Without loss of generality, we take the pressure in the reservoir to be zero.

Numerical Parameters

Our algorithm for integrating the reactive flow model uses four adjustable parameters: the spacing between grid cells along the X and Y axes (DX and DY); a parameter for adaptively controlling the size of the time step, DEL; and a convergence parameter for the time step iteration, EPS. The detailed use of these parameters has been described previously (Dembo et al., 1986).

The default values of numerical parameters in this study were $DX = DY = 9\mu$ (40×40 grid), $EPS = 10^{-3}$, and $DEL = 0.1$. Controls for accuracy were carried out by increasing and decreasing the numerical parameters as described previously (Dembo et al., 1986). In such benchmark tests, the effects of refinements in the numerical parameters were smaller in magnitude than effects caused by small perturbations to the initial conditions. The major systematic effect of refinement in spatial resolution was to increase the sharpness of gradients of network density. Thus our numerical solutions seem to represent smoothed or spatially averaged approximations to the underlying exact solutions.

Physical Parameters

In the reactive flow model the rheological and chemical properties of the cytoplasm are described by nine coefficients. (For the present study these are taken to be constant in space and time.) Before we compare the model with experiment, we desire to understand the consequences of taking any and all possible choices of these nine coefficients. We also need to consider various choices for the size and aspect ratio of the reaction vessel (L_y and L_x/L_y): a total of 11 independent variables (see Table I). To pursue this objective systematically, it is helpful to recognize and use relevant scaling laws and limiting cases of the reactive flow model. Two limiting cases are particularly important in this regard; the inviscid solution limit and the dilute network limit.

The inviscid solution limit is applicable provided that the two nondimensional quantities $(M_s + \Lambda_s)/(\phi L_y^2)$ and $(M_s + \Lambda_s)/(M_n + \Lambda_n)$ are both much less than $\tilde{\Theta}_n$. The dilute network limit requires not only these conditions but also that $2/\sigma \ll 1$. We have high confidence that both

limits are applicable in systems of biological interest (see Dembo and Harlow, 1986, for a detailed discussion of parameter estimates).

If we use both the inviscid solution limit and the dilute network limit and also introduce appropriate internal scales with respect to time, distance, density, and pressure, then we can reduce the effective dimensionality of parameter space from 11 to 5. As usual, the reduced parameter space can be expressed in terms of a set of nondimensional numbers. Except for changes of scale, any choice of physical parameter that gives the same nondimensional numbers will give the same performance of the reaction flow model. A convenient manner in which to choose the five fundamental nondimensional parameters is given in Table II.

Initial Conditions

We have carried out computations based on more or less baroque variations on two simple initial scenarios—the chemical equilibrium scenario and the mechanical equilibrium scenario.

In the chemical equilibrium scenario we assume that at the start of the reaction the network is uniformly distributed throughout the reaction vessel with density of $\tilde{\theta}_n$. Usually some sort of small perturbation is added to this basic distribution to simulate thermal fluctuations.

In the mechanical equilibrium scenario, we consider a cytoplasmic mass that is initially in the relaxed state (i.e., the mass is bathed in relaxation medium). We then suppose that a reaction is started by adding an appropriate amount of calcium to the medium. In setting up a particular calculation of this sort we must specify three pieces of information: (*a*) the initial configuration of the surface of the cytoplasmic mass, (*b*) the density of network within the cytoplasmic mass, and (*c*) what happens to change the stability of the relaxed state when calcium is added.

With reference to the reaction vessel discussed previously (see Fig. 2), we can specify the initial surface of the cytoplasmic mass by an arbitrary curve connecting the left and right boundaries. Below this curve we set the initial network density equal to some constant value; above the curve we set the starting network density equal to zero. For the most part we have investigated starting conditions in which the surface of the cytoplasmic mass is horizontal, with small vertical perturbations.

TABLE II
NONDIMENSIONAL PARAMETERS

Parameter	Symbol	Definition
Rending number	R^{ℓ}	$\Phi L_y^2/(2M_n + \Lambda_n)$
Density ratio*	D^{ℓ}	$\tilde{\theta}_n\sigma/2$
Contraction–reaction number	C^{ℓ}	$\Psi_F T_{eq}/(2M_n + \Lambda_n)$
Network viscosity ratio	V^{ℓ}	Λ_n/M_n
Reaction vessel aspect ratio	A^{ℓ}	L_x/L_y

*This terminology comes from the fact that $D^{\ell} \sim \tilde{\theta}_n/\hat{\theta}_n$ if σ is large (See Eq. 1b).

To specify the starting density of network within the cytoplasmic mass, we must make an interpretation of exactly what is meant by the "relaxed" state. First, consider the minimal properties of the relaxed state as documented by Taylor et al. (1973). (*a*) The relaxed state of cytoplasm is a state of mechanical equilibrium (i.e., a state in which the total kinetic energy is zero). (*b*) The contractile network in the relaxed state has a step function density distribution. (The network density is approximately constant within a well-defined region called the cytoplasmic mass and is approximately zero outside the cytoplasmic mass.) (*c*) The cytoplasmic mass in the relaxed state is "fluid" but maintains constant volume.

Fortunately, there is only one class of solutions of the reactive flow model that has the properties of the relaxed state. These solutions are the states of mechanical equilibrium that occur when an unreactive network shrinks or expands to the point where solvation stressed exactly counterbalance contractile stresses (see Dembo et al., 1986).

We conclude that in terms of the reactive flow model, one is forced to identify the relaxed state of Taylor et al. with the state of mechanical equilibrium of an unreactive network. It follows that the network density in a relaxed cytoplasmic mass can be computed by assuming a balance between solvation and contractile stresses. In more detail, the reactive flow model predicts that the network density in the initial cytoplasmic mass depends only on a quantity called the swelling number (σ) and that this density is given by the nontrivial root of the transcendental equation

$$\hat{\theta}_n + \sigma[\hat{\theta}_n + \ell n(1 - \hat{\theta}_n) = 0. \tag{1a}$$

For practical purposes the solution of Eq. 1a is given with sufficient accuracy by the Padé approximation

$$\hat{\theta}_n \sim (1 + 2\sigma) / (1 + \sigma)^2. \tag{1b}$$

To understand the role of calcium as the initiator of motility in demembranated cytoplasm, it is sufficient to consider the stability requirements of the initial state. According to the reactive flow model, the equilibrium state of an unreactive network will remain unchanged if and only if two conditions are met. First, the swelling number must remain constant so that Eq. 1a continues to be satisfied. Second, the network must remain unreactive (i.e., the relaxation time for the chemical reaction of network assembly and density, T_{eq}, must be effectively infinite). If we look at these stability conditions from the inverse point of view, we conclude that there are only two ways that the reactive flow model can explain the effect of calcium. (*a*) We can suppose that calcium causes a change in the swelling number, and (*b*) we can suppose that

calcium causes a decrease in the relaxation time. It is also possible that calcium should cause a change in both σ and T_{eq}.[2] Hypothesis *a* is equivalent to the assumption that the network remains unreactive both before and after the addition of calcium.

If this is the case, then the network simply undergoes a transient expansion or contraction leading from one equilibrium state to another. Such behavior is interesting and is certainly observed in demembranated cytoplasm (see Experimental Background). However, detailed calculations of transient contractions have been discussed by us in a previous publication (Dembo et al., 1986). Thus in referring to the mechanical-equilibrium scenario, we will restrict consideration to hypothesis *b*. In summary, this scenario assumes that, for negative times, T_{eq} is effectively infinite and that the density of network in the cytoplasm is equal to $\tilde{\theta}_n$. At $T = 0$, T_{eq} is suddenly lowered to a finite value in response to the addition of calcium.

RESULTS

We have carried out many numerical experiments using the various procedures outlined in the previous section. In all cases we find that during the initial phases of a computation the results depend strongly on the elapsed time. However, if computations are carried to sufficiently large times, then the results cease to evolve in time.[3]

Factors can be grouped according to the importance of their influence on the long-term behavior of the model. For example, the exact choice of initial condition has a relatively minor effect on results after sufficiently long times. Similarly the treatment of the boundary conditions, the choice of numerical parameters, the aspect ratio of the reaction vessel, and the network viscosity ratio all were rather subtle in their effects on long-term behavior. These observations led us to divide our investigation into two phases. In phase 1 we held all factors fixed except for the rending number, the contraction–reaction number, and the density ratio. In phase 2 we allowed the secondary factors to vary so as to observe modifications to the results obtained in phase 1.

In phase 1 studies, we used the hard-wall method for the top boundary condition, mirror symmetry conditions on the left and right sides, and stagnation conditions at the lower boundary. Both the aspect ratio of the reaction vessel (L_x/L_y) and the network viscosity ratio (Λ_n/M_n) were set equal to one. The initial conditions consisted of a mechanical equilibrium scenario with horizontal interface and superimposed sinusoidal perturbation. The average height of the interface was equal to the product of L_y and the density ratio. This ensures that the average density of network in the reaction vessel at the start of the reaction is $\sim \tilde{\theta}_n$. The maximum amplitude of the perturbation was 30% of the average interface height, the phase was equal to $\pi/2$, and the wave length was equal to $2L_x$. The solutions obtained under such default conditions could be organized into five classes according to increasing degrees of dynamical complexity.

Class A. At long times the system approaches a state of complete chemical equilibrium. This means that the network density is equal to $\tilde{\theta}_n$ at all points in the reaction vessel, the pressure is everywhere constant, and all components of velocity for both solution and network vanish.

Class B. At long times the system approaches a state of chemical equilibrium except in a thin layer adjacent to the top boundary of the reaction vessel.

Class C. At long times the system approaches a unique steady state that is far from chemical equilibrium. In this steady state horizontal components of velocity are zero, and the network density is monotone decreasing from the bottom to the top of the reaction vessel.

Class D. Type D dynamics fall in the grey area between types C and E. In type C dynamics the behavior of the reactive flow model at long times is simple, unique, and deterministic. In type E dynamics the behavior of the model at long times is chaotic. In the D-type dynamical regime, simple solutions of type C are not stable, and yet the behavior of the model is not yet sufficiently complex as to be chaotic. Thus we define type D in negative terms. This is admitedly rather unsatisfactory, but the situation will hopefully become clearer as we discuss specific examples.

Class E. At long times the system follows a slow aperiodic tragectory through a manifold of structurally similar unstable states (i.e., a strange attractor).

TABLE III
DYNAMICAL MODES PRODUCED IN VARIOUS SUBREGIONS OF PARAMETER SPACE*

	Nondimensional variable		
	R^ℓ	C^ℓ	D^ℓ
A	$0 < R^\ell$	$0 < C^\ell$	$1 < D^\ell$
B	$0 < R^\ell$	$C^\ell < (1 - D^\ell)^{-2}$	$D^\ell < 1$
C	$0 < R^\ell < R_{CD}$	$(1 - D^\ell)^{-2} < C^\ell$	$D^\ell < 1$
D	$R_{CD} < R^\ell < R_{DE}$	$(1 - D^\ell)^{-2} < C^\ell$	$D^\ell < 1$
E	$R_{DE} < R^\ell$	$(1 - D^\ell)^{-2} < C^\ell$	$D^\ell < 1$

*A^ℓ and V^ℓ are both equal to 1. Other default conditions for phase 1 also hold.

[2]Calcium might or might not affect other parameters such as the network viscosities. Such effects are not relevant in the present context since they would not cause a destabilization of the equilibrium state.

[3]We use the term "evolve" advisedly. For example, a system in periodic motion or turbulent motion does not evolve.

The various dynamical categories are caused by different choices of the fundamental nondimensional numbers as summarized in Table III. Due to the purely empirical basis for the classifications, there is an inevitable ambiguity as to where to draw the line between some of the classes. Except for such semantic difficulties, the various categories we have described cover the whole of the three-dimensional parameter space spanned by $C^\#$, $R^\#$, and $D^\#$.

We refer to dynamical classes A and B as cases of trivial dynamics. Class A is characterized by a density ratio greater than one. This means that at chemical equilibrium the network tends to expand rather than contract. Thus, existing network swells and new network is synthesized until the entire reaction vessel is uniformly filled. At this point further expansion is prevented by the boundaries. In class B dynamics the network tends to contract at chemical equilibrium, but this contraction is effectively counteracted by the chemical reaction. The result is that chemical effects dominate mechanical effects, and the network density remains very close to chemical equilibrium except in a thin boundary layer at the top of the reaction vessel. This boundary layer occurs because there is always a slight tendency for network to retract from a no-stick surface. For the remaining three dynamical classes (C, D, and E), the product $C^\#(1 - D^\#)^2$ is larger than one and $D^\#$ is smaller than one. Both of these elements are necessary to obtain nontrivial results.

Detailed physical and numerical parameters for various computations of type C, D, and E are summarized in Table IV. The nodal computation of type C is designated C_1. Other type C computations are designated C_2, C_3, etc. Computations of types D and E listed in Table IV are designated D_1, D_2, ... and E_1, E_2, ..., respectively. Note that Table IV gives the full complement of independent variables actually used in various computations. This is done for thoroughness even though some of the parameters are irrelevant (see preceding discussion on parameter space). Nondimensional numbers corresponding to each computation can be computed using the definitions in Table II.

Fig. 3 *A* is a computer-generated image illustrating the final steady state in computation C_1. Within this figure the effective pressure field, the network density field, the network velocity field, and the solution velocity field are displayed by four subplots. The physical time in seconds is written at the top-center of each figure. To the left of each subplot is an abbreviated label indicating its content. The label on each subplot is followed by a semicolon and a numerical scale parameter written in FORTRAN E format. As described below, these scale parameters allow quantitative interpretation of the various subplots.

The top-left subplot in Fig. 3 *A* gives a color-contour map of the natural logarithm of the normalized network volume fraction. The reference contour in this map (blue contour line drawn in triple thickness) is taken at $\ell n\,(\theta_n/\theta_0) = 0$. The scale parameter to the left of the subplot indicates the value of the normalization constant, θ_0. Contour lines in this plot are spaced at half-log intervals: $\ell n(\theta_n/\theta_0) = 0, \pm \frac{1}{2} \pm 1 \pm \frac{3}{2}, \ldots$ Contour lines that fall in the range $10^{-2} < \theta_n/\theta_0 < 10^{-1}$ are colored green; lines in the range $10^{-1} < \theta_n/\theta_0 < 1$ are colored yellow; the reference contour is colored blue; lines in the range $1 < \theta_n/\theta_0 < 10$ are colored red; and lines in the range $10 < \theta_n/\theta_0 < \infty$ are colored magenta.

To avoid the distracting clutter produced by contour lines corresponding to extremely low densities, we delete contour lines below a certain cutoff. Unless otherwise noted, the cutoff is set at a level 100-fold smaller than θ_0.

In the present study we consistently take the scale

TABLE IV
PARAMETERS OF SELECTED COMPUTATIONS*‡§

	$\tilde{\theta}_n$	T_{eq}	Ψ_F	σ	M_n	Λ_n	M_s	Λ_s	Φ	L_x	L_y
		s	*dyn/cm²*		*P*	*P*	*P*	*P*	*P/cm²*	*cm*	*cm*
Computations											
C_1	1.0×10^{-3}	1.5×10^{1}	6.0×10^{4}	4.0×10^{2}	2.0×10^{4}	2.0×10^{4}	1.0×10^{-2}	1.0×10^{-2}	1.0×10^{8}	3.6×10^{-2}	3.6×10^{-2}
C_2	1.0×10^{-3}	3.0×10^{1}	6.0×10^{4}	4.0×10^{2}	2.0×10^{4}	2.0×10^{4}	1.0×10^{-2}	1.0×10^{-2}	1.0×10^{8}	3.6×10^{-2}	3.6×10^{-2}
C_3	1.0×10^{-3}	3.0×10^{1}	6.0×10^{4}	8.0×10^{2}	2.0×10^{4}	2.0×10^{4}	1.0×10^{-2}	1.0×10^{-2}	1.0×10^{8}	3.6×10^{-2}	3.6×10^{-2}
E_1	1.0×10^{-3}	3.0×10^{1}	6.0×10^{4}	4.0×10^{2}	2.0×10^{4}	2.0×10^{4}	1.0×10^{-2}	1.0×10^{-2}	1.0×10^{10}	3.6×10^{-2}	3.6×10^{-2}
E_2	1.0×10^{-3}	3.0×10^{1}	6.0×10^{4}	1.0×10^{3}	2.0×10^{4}	2.0×10^{4}	1.0×10^{-2}	1.0×10^{-2}	2.0×10^{10}	3.6×10^{-2}	3.6×10^{-2}
E_3	1.0×10^{-3}	3.0×10^{1}	6.0×10^{4}	1.0×10^{2}	2.0×10^{4}	2.0×10^{4}	1.0×10^{-2}	1.0×10^{-2}	2.0×10^{10}	3.6×10^{-2}	3.6×10^{-2}
D_1	1.0×10^{-3}	3.0×10^{1}	6.0×10^{4}	6.0×10^{2}	2.0×10^{4}	2.0×10^{4}	1.0×10^{-2}	1.0×10^{-2}	1.0×10^{9}	3.6×10^{-2}	3.6×10^{-2}
D_2	1.0×10^{-3}	2.5×10^{1}	6.0×10^{4}	4.0×10^{2}	2.0×10^{4}	2.0×10^{4}	1.0×10^{-2}	1.0×10^{-2}	1.0×10^{9}	3.6×10^{-2}	3.6×10^{-2}
D_3	1.0×10^{-3}	3.0×10^{1}	6.0×10^{4}	4.0×10^{2}	2.0×10^{4}	2.0×10^{4}	1.0×10^{-2}	1.0×10^{-2}	0.7×10^{9}	3.6×10^{-2}	3.6×10^{-2}
D_4	1.0×10^{-3}	3.0×10^{1}	6.0×10^{4}	4.0×10^{2}	2.0×10^{4}	2.0×10^{4}	1.0×10^{-2}	1.0×10^{-2}	1.0×10^{9}	3.6×10^{-2}	3.6×10^{-2}
D_5	1.0×10^{-3}	9.0×10^{1}	6.0×10^{4}	4.0×10^{2}	2.0×10^{4}	2.0×10^{4}	1.0×10^{-2}	1.0×10^{-2}	1.0×10^{9}	3.6×10^{-2}	3.6×10^{-2}
D_6	1.0×10^{-3}	9.0×10^{1}	6.0×10^{4}	6.0×10^{2}	2.0×10^{4}	2.0×10^{4}	1.0×10^{-2}	1.0×10^{-2}	1.0×10^{9}	3.6×10^{-2}	3.6×10^{-2}

*Default boundary conditions: hard-wall method for the top boundary, zero flux at the lower boundary, and mirror symmetry at the left and right boundaries.

‡Default initial conditions: mechanical equilibrium scenario. The initial surface of the cytoplasmic mass was flat with small verticle perturbations.

§Default numerical parameters: $DX = DY = 9 \times 10^{-4}$ cm (i.e., 40 × 40 grid), $EPS = 10^{-3}$, $DEL = 0.1$.

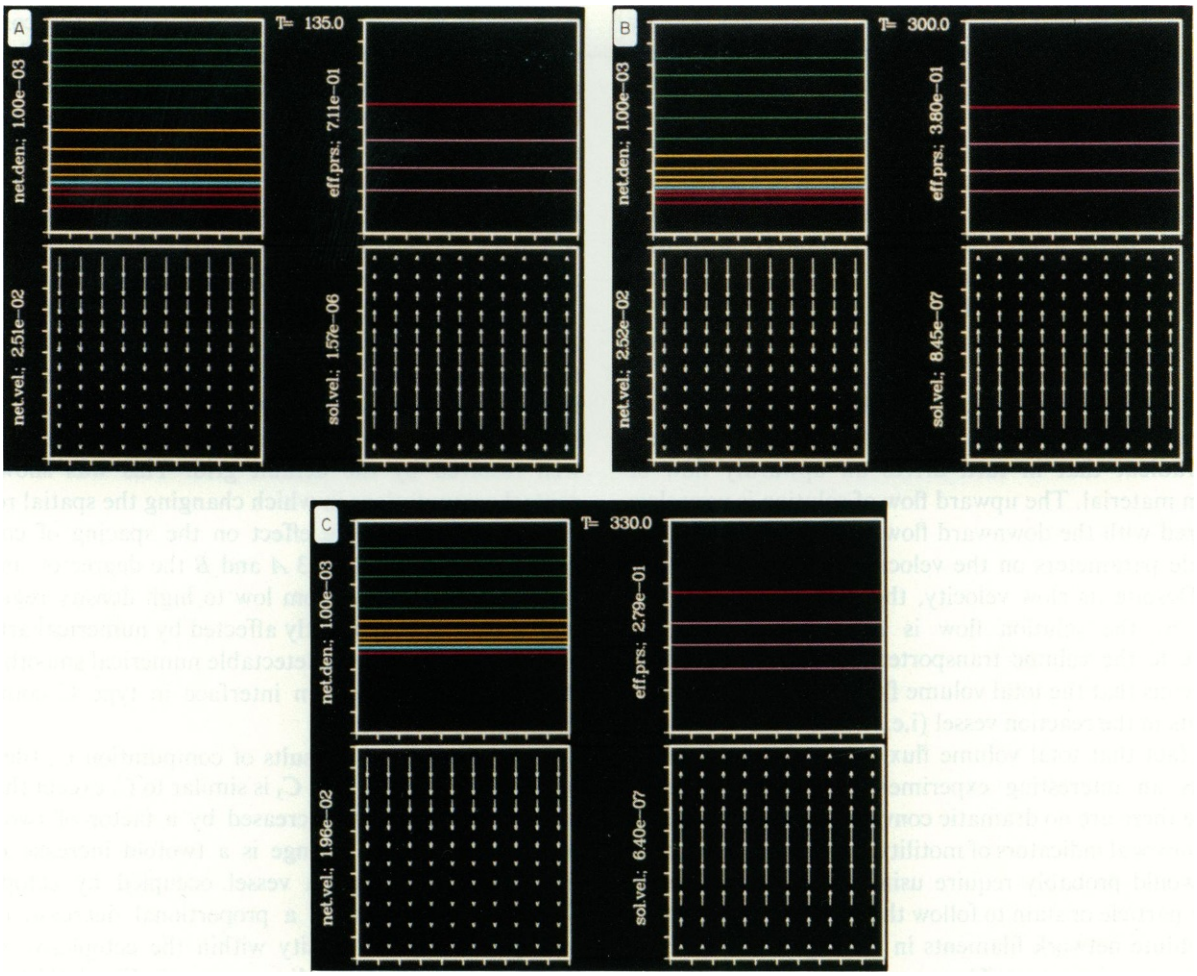

FIGURE 3 The C-mode. *A–C* show the solutions obtained at long times in computations C_1, C_2, and C_3 (detailed parameters are given in Table IV), respectively. All cases of the C mode are characterized by a completely stable and unique final state. In this final state the network density distribution decreases in a monotone fashion from the bottom to top of the reaction vessel. Solutions are independent of the horizontal coordinate, and horizontal components of velocity vanish. If the C' is much greater than one, then the reaction vessel can be approximately divided into subregions of endoplasm and ectoplasm. Increasing the C' causes an increase in the density gradients at the interface between endoplasm and ectoplasm without changing the position of the interface (compare C_1 and C_2). Increasing the D' causes an expansion of the ectoplasmic volume and simultaneously decreases the maximum density within the ectoplasm (compare C_2 and C_3).

parameter of network density contour plots equal to the chemical equilibrium density (i.e., $\theta_0 = \tilde{\theta}_n$). This means that regions of a reaction vessel enclosed by the reference contour correspond to regions where the balance of chemical reaction favors breakdown of network. Below the reference contour, the balance of chemical reaction favors formation of network.

The top right subplot in Fig. 3 *A* gives a color contour map of the effective pressure field. The scale parameter to the left of the pressure subplot gives the spacing between pressure contours in dynes /cm^2. In most figures the reference contour $P_F = 0$ is shown as a thick blue line. However, in Fig. 3 *A* the zero pressure contour is not visible because it coincides with the top boundary of the reaction vessel. In cases where hard-wall boundary conditions are used, the pressure field is normalized so that the mean pressure acting on the upper boundary is zero. This means that contour lines corresponding to negative pressure do not occur.

The lower left subplot in Fig. 3 *A* is a vector map of the network velocity field. In producing this map, vectors are drawn emanating from various evenly spaced points throughout the reaction vessel. The direction of the arrowhead on each vector shows the direction of network flow, and the length of the tail of the arrow is proportional to the speed of flow (if the speed is very slow, then the tail is not visible.) The scale parameter to the left of the subplot gives the speed in centimeters per second corresponding to an arrow of standard length. The standard length is equal to the spacing between the tick marks that border the subplot. The magnitude of the scale parameter is adjusted internally so as to prevent neighboring arrows from overlapping.

The lower right subplot in Fig. 3 *A* is a vector map of the

solution velocity field. The format of the solution velocity map is the same as for the network velocity map except that the scale parameter on the two subplots is usually different.

The basic behavior illustrated by Fig. 3 *A* is typical of all class C computations. In the upper portion of the reaction vessel (yellow and green contour lines) the network density is below $\tilde{\theta}_n$. In the lower portion (red contours) the density is above $\tilde{\theta}_n$. On balance, network is formed in the upper regions of the vessel, and contractile stresses pull the network down towards the lower regions where it is broken down.

As a result of the incompressibility constraint, the downward flow of network creates a countervailing pressure gradient that in turn drives an upwardly flow of solution material. The upward flow of solution is very slow compared with the downward flow of network. (Compare the scale parameters on the velocity vector maps in Fig. 3 *A*). Despite its slow velocity, the actual volume transported by the solution flow is everywhere equal and opposite to the volume transported by the network flow. This means that the total volume flux is identically zero at all points in the reaction vessel (i.e., $\theta_s\Omega_s + \theta_n\Omega_n = 0$).

The fact that total volume flux is zero in the C mode presents an interesting experimental difficulty. This is because there are no dramatic convection currents to serve as unequivocal indicators of motility. To demonstrate the C mode would probably require using some sort of special marker particle or stain to follow the steady inward motion of the dilute network filaments in the region surrounding the cytoplasmic mass. These considerations may help explain why C-type dynamics were not observed by Taylor et al. or by Kuroda.

Fig. 3 *B* shows the results of computation C_2 (detailed parameters in Table IV). C_2 is similar to C_1 except that the contraction–reaction number, $C^\#$, is increased by a factor of two. This change causes contour lines corresponding to low network densities to be displaced downward while lines corresponding to high densities are displaced upwards. Thus the gradient of network density at the interface between the low and high density regions greatly increases, but the position of the interface and the value of the maximum density remain the same. If the contraction–reaction number is further increased, the network density distribution more closely approaches a step function. If the contraction–reaction number is decreased, gradients of network density decrease gradually until $C^\# (1 - D^\#)^2$ equals one. At this point there is a transition to class B dynamics.

Both computations C_1 and C_2 are characterized by a rather sharp division of the reaction vessel into regions of high and low network density. This dynamical feature occurs irrespective of dynamical class provided the $C^\#$ is much greater than 1. (In practice a $C^\#$ of 10 or larger is usually sufficient.) The sharp distinction between regions of high and low network density predicted by the reactive flow model may provide an explanation of the common cytological observation of distinct regions of endoplasm and ectoplasm. Whether or not this proposal is correct, it is convenient to use cytological nomenclature. We will thus refer to the portions of a reaction vessel where the network density approximates $\hat{\theta}_n$ as ectoplasmic regions. We will refer to regions of low density as endoplasmic regions. We will never use these terms to refer to material in the "inner" and "outer" portions of the reaction vessel.

The degree of sharpness of the density gradient observed at an endoplasm–ectoplasm interface can be affected by the choice of numerical parameters (see section on numerical parameters). Thus it is important to point out that in the case of computations C_1 and C_2, the gradients are very well resolved by the default grid. This was shown by control computations in which changing the spatial resolution had no detectable effect on the spacing of contour lines. Therefore, in Fig. 3 *A* and *B* the degree of smoothness of the transition from low to high density regions is real and is not significantly affected by numerical artifact. The default grid causes detectable numerical smoothing of the endoplasm–ectoplasm interface in type C computations only if $C^\# \gtrsim 60$.

Fig. 3 *C* shows the results of computation C_3 (detailed parameters in Table IV). C_3 is similar to C_1 except that the value of $D^\#$ has been increased by a factor of two. One consequence of this change is a twofold increase in the fraction of the reaction vessel occupied by ectoplasm. Simultaneously there is a proportional decrease in the maximum network density within the ectoplasm. (Note that only one red contour line appears in Fig. 3 *C*.) In other words, the total mass of network in the ectoplasmic region remains the same, but the volume occupied by the region has been increased.

In all three computations discussed thus far, it can be verified that the fraction of the reaction vessel occupied by ectoplasm in the final state is very close to the value of the density ratio. This observation turns out to be quite general (see Appendix B for a derivation).

The general correlation between density ratio and the fraction of ectoplasm provides a simple experimental means of determining the density ratio. For example, from Fig. 1 *A* it can be seen that the volume of the central ectoplasmic region can be approximated by a sphere. For the volume of the reaction vessel, we take a sphere at the same center that includes the outermost extent of mixing and disturbance caused by the reaction. Such a sphere has radius of two or possibly three times the radius of the ectoplasm. We thus conclude that to simulate this experiment using the reactive flow model, we must use a density ratio of between $(\frac{1}{2})^3$ and $(\frac{1}{3})^3$. In a two-dimensional analysis of the experiment, the appropriate density ratio is in the range $(\frac{1}{2})^2$–$(\frac{1}{3})^2$.

Fig. 4, *A–C* illustrates some cases of class E dynamics (computations E_1, E_2, and E_3). In both classes E and C, the boundary and initial conditions predispose the network to

FIGURE 4 The E mode. *A–C* show the solutions obtained at long times in computations E_1, E_2, and E_3, respectively (detailed parameters are given in Table IV). All cases of the E mode are characterized by a chaotic or aperiodic final state in which the flow and distribution of network and solution phases constantly change. E_1 represents a case with rending number of 216 and density ratio of 0.2. For these parameters large amorphous blobs or clumps of ectoplasm of constantly varying shape and position are suspended in streams of vigorously flowing endoplasm. E_2 shows a case with rending number of 432 and density ratio of 0.5. For such parameters endoplasm is confined to a system of branching channels that cut through the ectoplasmic material. In contrast, E_3 shows a case with rending number of 432 and density ration of 0.05. As in the case of type C computation, decreasing the density ratio decreases the proportion of ectoplasm while increasing the maximum density.

retract from the top boundary and to stick to the lower boundary. The new element in class E is the fact that localized lateral contractions are now fast compared with motion along the vertical axis. Thus, the network in the upper regions of the reaction vessel collects into a number of amorphous clumps or blobs of ectoplasm before reaching the lower regions. Each of these ectoplasmic blobs is suspended in violent currents of streaming endoplasmic material. Each blod acts as an independent focus for local contractile activity; network material is added by accretion to the periphery of the blob and lost due to chemical breakdown in the interior. The original ectoplasmic material of the cytoplasmic mass has been absorbed into the suspended ectoplasmic clumps. Only a thin layer of material and a few adherent clumps remain at the bottom of the reaction vessel. The latter are probably artifacts caused by the bottom boundary condition. All but a faint semblance of vertical polarity, so prominent in class C dynamics, has been lost.

In all cases of class E dynamics, the dynamical state at long times is turbulent or chaotic. This means that on a slow time scale the dynamical state continuously changes in a random non-evolutionary fashion. Some of the ectoplasmic blobs grow; others shrink; all slowly tumble and rotate. Occasionally two clumps come too close together and fuse. Occasionally a large gap develops between neighboring clumps, and a new clump spontaneously forms to fill the void. Occasionally a very large clump will undergo fission. In short, the details are constantly changing but, in a time-averaged or probabilistic sense, the basic situation remains constant. In terms of the jargon of dynamical systems theory, one would say that the strange attractor was of low dimensionality with respect to the phase space.

If the contraction–reaction number is large compared to one, then class E computations display a strong endoplasm–ectoplasm differentiation. As in all such cases, the percentage of ectoplasm is approximately equal to the density ratio even though the disposition and organization of the ectoplasm is constantly changing. In computation E_1, ectoplasm fills ~20% of the reaction vessel. Computation E_2 illustrates what happens when there is 50% ectoplasm (Fig. 4 *B*). As can be seen, if both rending number and percent ectoplasm are high, then the random flows of solution material become confined to a branching and anastomosing network of channels. In computation E_3, there is only 5% ectoplasm. In this case, the majority of the reaction vessel is filled by endoplasm, with uniformly scattered foci of very dense ectoplasm.

It is difficult to resist noting the similarity between solutions of the type shown in Fig. 4 *B* and the well-known cytoplasmic organization of *Physarum polycephalum*. This similarity, though suggestive, does not extend to the periodic flow patterns observed in *Physarum* (i.e., shuttle streaming). In the reactive flow model the endoplasmic flow, though confined to channels at high $D^\#$, is nonetheless aperiodic and has only short range spatial correlations. Some additional factor (e.g., a chemical oscillator) is probably necessary to bring order out of chaos.

Starting with parameter values that yield type C dynamics, one can obtain type E dynamics by increasing the value of the rending number, leaving the density ratio and the contraction–reaction number fixed (compare computations C_2 and E_2). This means that by progressively increasing the value of the rending number, one can study the so-called "path to chaos." Such studies have become fashionable in recent years because they sometimes reveal universal features such as the well-known period doubling cascade (Feigenbaum, 1980).

We are loath to be fashionable, but it is nevertheless true that progressive variation of the rending number at fixed density ratio and contraction–reaction number is a natural and systematic approach to exploring the complexities of type D behavior. By such studies we find that for fixed initial conditions there is always a very sharp threshold for the transition from class C to class D. We denote the threshold value of the rending number for the C → D transition by R_{CD}. We have determined the value of R_{CD} by a series of numerical experiments for various values of $C^\#$ and $D^\#$. Within the error of these calculations, R_{CD} does not seem to depend on the $C^\#$. R_{CD} is weakly dependent on $D^\#$ if $D^\#$ is small, but $R_{CD} \to \infty$ as $D^\# \to 1$. Note that if $C^\# (1 - D^\#)^2 \lesssim 1$, then the dynamical class is independent of the rending number (i.e., class B cannot progress to class D).

After the sudden onset of type D behavior, further increases in the rending number at first produce smooth variations in dynamical behavior. In this interval, increasing the rending number causes the long-term dynamical state of solutions to become more and more complicated by

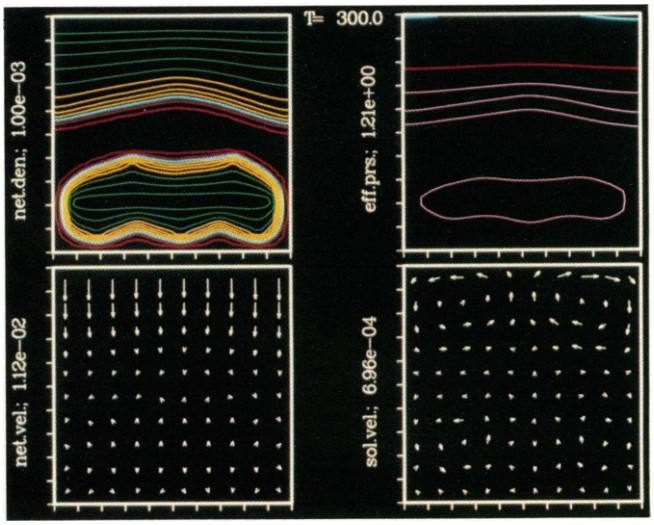

FIGURE 5 The crypt subtype. The final steady state in computation D_1 is shown. Crypts or vacuoles of endoplasm surrounded by ectoplasm are a commonly found subtype of the D mode. This subtype is favored at intermediate values of $C^\#$, particularly if $D^\#$ is large.

a series of small transitions. Eventually, if the rending number is made large enough, one obtains fully developed class E dynamics. We surmise from these observations that there exists a value of the rending number, R_{DE}, at which a D → E transition occurs.

Precise determination of R_{DE} requires use of some quantitative measure of the degree of chaos (e.g., power spectrum or Lyapunov exponent). For the present study, there seems little to be gained by using such measures since they are expensive and since we are aware of no cases where they significantly contradict or expand one's quali-

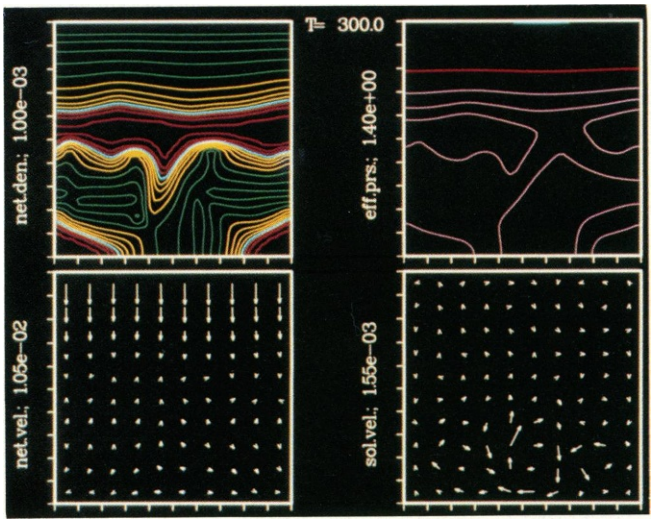

FIGURE 6 The layer subtype. The final state in computation D_2 is illustrated. A layer of ectoplasm suspended in the middle of the reaction vessel frequently occurs in type D solutions if the $C^\#$ is not too large. In the case shown, the solution is not steady but demonstrates complex waves of contraction that pass back and forth across the suspended layer.

tative impression of random versus orderly behavior. On such a qualitative basis we find that the range of type D behavior spans no more than a factor of five in the rending number (i.e., $1 \leqq R_{DE}/R_{CD} \leqq 5$). The ratio R_{DE}/R_{CD} approaches its lower limit as $C^\sharp \rightarrow (1 - D^\sharp)^{-2}$ and approaches its upper limit as $C^\sharp \rightarrow \infty$.

Within the general category of class D solutions, we have observed three subtypes based on the morphology of the endoplasm–ectoplasm distribution. These subtypes are called crypts, layers, and fortifications. Fig. 5 shows an example of a layer-type solution (computation D_1); Fig. 6 shows a case of a crypt-type solution (computation D_2); and Fig. 7, *A–D* show some cases of fortification-type solutions (computations D_3–D_6). Parameter values for these various computations are listed in order of appearance in Table IV.

It can be verified that the length of the endoplasm–ectoplasm boundary in a D-type solution is always greatly increased relative to the underlying C-type solution. At the same time the volume of the endoplasmic and ectoplasmic regions in the two sorts of solutions remains approximately the same (compare Fig. 7, *A* and *B* with 3 *B*). Fortifications, crypts, and layers simply represent several topologically distinct mechanisms for producing this sort of change. This observation is quite revealing as to the underlying physical factors that cause the breakdown of the C mode. The instability seems to be driven by the need to make a shorter path for the outflow of solution material from the interior of the ectoplasmic mass. Alternatively, one could say that the transition is driven by the need to relieve the buildup of pressure inside the ectoplasmic areas.

Kinetically, the crypt subtype (Fig. 5) frequently occurs by growth of point-like defects in the ectoplasmic layer. Ectoplasm retracts away from such points in a motion that resembles the tearing of a stretched fabric. Retraction of the ectoplasm ultimately results in an observable crypt. As the crypt grows in size, the stresses driving the instability are gradually relieved, and the situation finally reaches a stable equilibrium. The example shown in Fig. 5 represents a single very large crypt formed by fusion of three smaller crypts. The solution shown is a completely stable steady

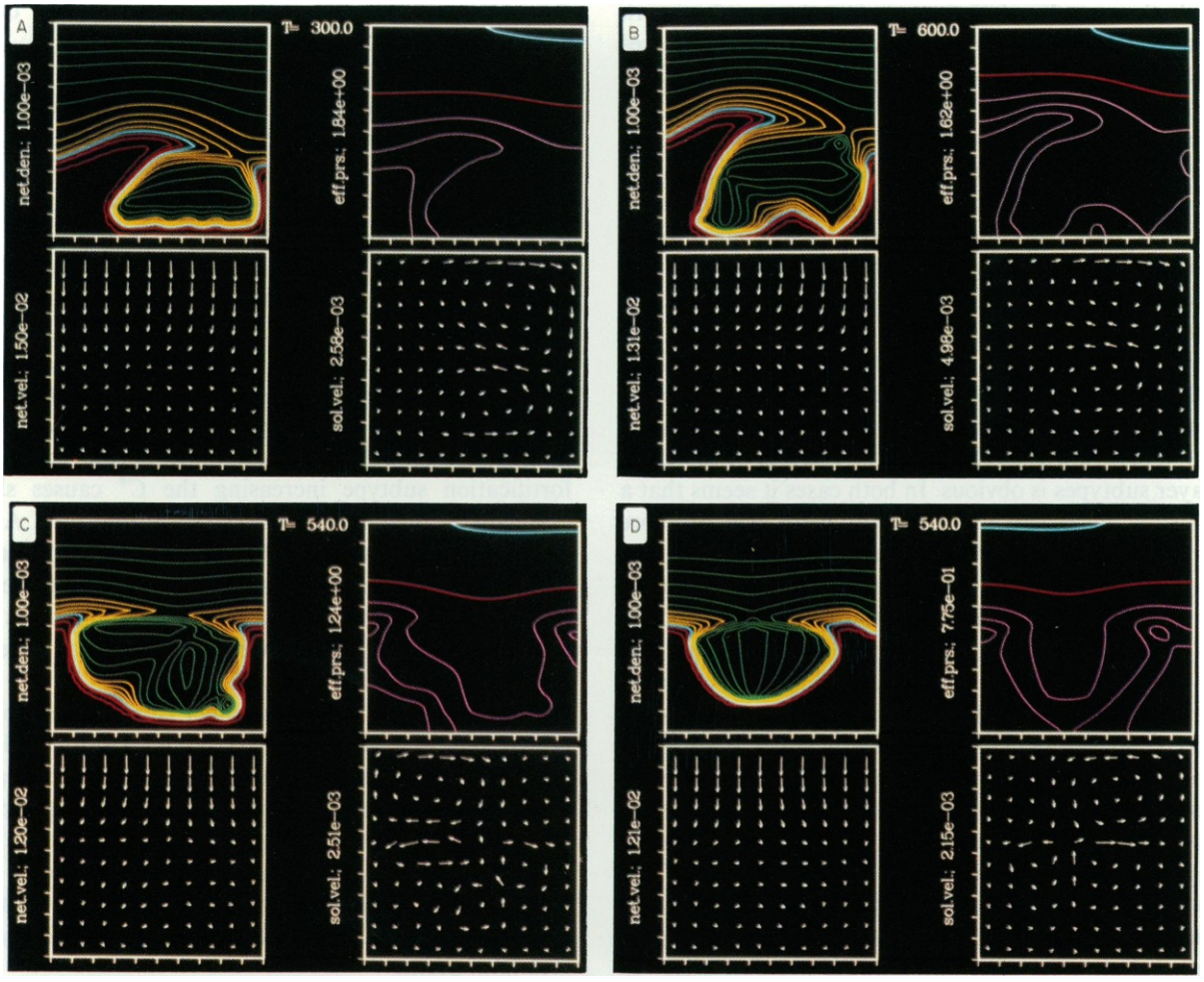

FIGURE 7 The fortification subtype. *A–D* illustrate the final steady states in computations D_3, D_4, D_5, and D_6, respectively. Comparison of D_3 and D_4 illustrates the effect of increasing $R^\sharp$. Comparison of D_4 and D_5 illustrates the effect of increasing $C^\sharp$. Comparison of D_5 and D_6 illustrates the effect of increasing $D^\sharp$.

state. In other cases, particularly if $D^{\#} \rightarrow 1$, a number of small crypts can be scattered at various points.

Outwardly, the main observable consequence of the crypt subtype is a bulging of the surface of the cytoplasmic mass at points overlying each crypt. Such bulges lead to vigorous eddies or convective cells in the endoplasmic material outside the cytoplasmic mass (Fig. 5, lower left). In calculations that use the reservoir method for the top boundary condition, it can be shown that such convection cells will extend for hundreds of microns into the outer solution and can have very fast flow velocities (c.f., phase II computations). It therefore seems possible that the rossette phenomenum observed by Kuroda can be explained as a manifestation of the crypt subtype of the D mode.

In support of this view, we note that if one looks carefully at the edge of the cytoplasmic mass in Fig. 1 *B*, one can detect what appear to be small bumps or blebs.

The layer subtype is simply a special case of the crypt subtype in which the crypts grow and fuse with each other to the point where they completely span the reaction vessel from left to right. Layers can also form by direct fusion of clumps in the upper part of the reaction vessel. In the example shown in Fig. 6 there are a few clumps of network remaining attached to the lower boundary. In other cases the lower boundary is completely covered by a continuous layer of ectoplasm.

The layer subtype is very stable and uniform at low values of the $C^{\#}$ (i.e., values less than ~ 15). At large values of the $C^{\#}$, layer solutions are subject to complex limit cycle oscillations, indicating that they are of marginal stability (the example shown in Fig. 6 is such a case). At even larger values of $C^{\#}$, layers will, in fact, break apart into separate clumps.

In a three-dimensional system, the layer subtype of the type D mode would correspond to a thick spherical shell of ectoplasm completely surrounding a central core of endoplasm. When viewed in this way, the relation of the crypt and layer subtypes is obvious. In both cases it seems that a cytoplasmic mass can swell and fill with one or more internal pockets of endoplasm like a balloon. This is rather a dramatic prediction of the reaction flow model, but we know of no experimental observations that might correspond to such a structure. This may be because crypts and layers are unstable in three-dimensional space. Nevertheless, it would be of interest to somehow fix and section some dissociated masses of cytoplasm to see whether or not crypt and/or layer solutions can occur experimentally.

Kinetically, fortification solutions occur in three ways. Crypts can develop breaks in their top surface, creating a passage for flow of solution out of the interior of the cytoplasmic mass. Alternatively, clumps can form in the region outside the cytoplasmic mass. Such clumps can then be pulled downward until they contact and fuse with the surface. Finally, small perturbations in the surface of the cytoplasmic mass can grow by accretion or retraction until large prominences and/or cavities develop. In all three cases the final result is the same.

Consider the general similarities of type D solutions that have the fortification morphology. In common with class C computations, there is a strong top-to-bottom polarity in the reaction vessel. Network is synthesized in the upper regions of the vessel and flows downward due to contractile stresses. In the ectoplasmic regions at the bottom of the reaction vessel, the network is disassembled for recycling. In common with class E computations, contractile stresses produce some tendency for the network to aggregate laterally as it flows downward. However, instead of forming disconnected blobs, the network collects into arching ectoplasmic protrusions. Within the protrusions, the network continues to flow downward toward the main cytoplasmic mass, but at a greatly reduced speed.

Because of the relatively high network density, the drag force acting on the solution phase within ectoplasmic protrusions is large. This causes both network and solution within protrusions to flow in the same direction with almost the same speed. Thus, unlike the case of class C motion, the volume flux does not vanish at all points. Channels of downward volume flux follow the protrusions of high network density.

To satisfy the condition of incompressibility, it is necessary to balance the channels of downward volume flux by channels of upward flux. When network material moves laterally to form ectoplasmic protrusions, regions that are somewhat depleted in network remain behind. Thus, between the ectoplasmic protrusions there are cavities of endoplasm that offer reduced hydraulic resistance to the passage of solution. In response to the high pressure at the base of the reaction vessel, the upward flow of solution through these endoplasmic cavities is quite fast.

The detailed form and behavior of fortification, crypt, and layer solutions can be predictably altered by variations in $C^{\#}$, $D^{\#}$, and $R^{\#}$. For example, in the case of the fortification subtype increasing the $C^{\#}$ causes sharper gradients at the endoplasm–ectoplasm interface. A sharp interface can support fine details such as sharp corners, bumps, and indentations. Large values of $C^{\#}$ also decrease the height of protrusions and increase the thickness of the ectoplasmic layer at the lower boundary (compare Figs. 7, *B* and *C*).

Increases in the rending number cause the ectoplasmic protrusions to become longer, more vertical, and more closely spaced (compare *A* and *B* of Fig. 7). If the value of $R^{\#}$ is close to R_{DE}, then the ectoplasmic protrusions become unstable and tend to pinch off at the tips. If this happens, clumps of ectoplasm can be suspended in the outer portions of the reaction vessel overlying the typical fortification pattern. Such hybrid solutions display complex limit cycles.

Fig. 7 *D* illustrates the characteristic form of the fortification subtype when the value of $D^{\#}$ is large (compare *C*

and D of Fig. 7). This illustration is interesting because the protrusions of ectoplasm are little more than small bumps while the endoplasmic pocket remains wide and deep. As in the case of the crypt solutions, unless sections are taken, the only manifestation of such a solution would be the eddies of flowing endoplasm that lie outside the cytoplasmic mass.

In the results discussed thus far, all factors except for the primary nondimensional numbers $C^\#$, $R^\#$, and $D^\#$ have taken their default or phase I values. We will now consider the effect of secondary factors. These secondary factors are: the initial conditions, the boundary conditions, the aspect ratio of the reaction vessel ($A^\#$), and the viscosity ratio ($V^\#$). As far as we can tell from our numerical studies, these latter factors have negligible effects except under circumstances where the balance of primary factors is close to a turning point. Thus for the most part, if $C^\#$, $R^\#$, and $D^\#$ are fixed, then a type A, B, C, D, or E computation will remain of the same type no matter how one varies the secondary factors. On the other hand, secondary factors can cause changes in the detailed features of a computation; for example, changes in initial conditions can affect the subtype of a type D computation.

Initial conditions can also affect the transition from the C mode to the D mode. In other words, the values of R_{CD} given in Table V refer only to a particular initial condition. By changing the initial condition, it is possible to increase or decrease the value of R_{CD} by up to a factor of two. This effect is most pronounced when the $C^\#$ is large (i.e., $C^\# \gtrsim 30$). We conclude that for large $C^\#$, there is a range of $R^\#$ such that both the C mode and the D mode are locally stable. In this range the C mode will break down only if a sufficiently large perturbation of appropriate wavelength is imposed (the default initial conditions are close to optimal for breakdown of the C mode). This makes a testable experimental prediction: that under slightly subcritical conditions a moderate mechanical perturbation such as pricking with a needle or sucking with a micropipette can induce or "excite" a transition from a state of low or invisible activity (i.e., the C mode) to a state of high activity (i.e., flaring).

TABLE V
CRITICAL POINTS FOR THE C → D TRANSITION*

	$D^\#$			
R_{CD}‡	0.1	0.2	0.4	0.8
$C^\#$				
3	11.5 ± 2	15.1 ± 2	∞	∞
10	11.5 ± 2	15.1 ± 2	23.8 ± 2	∞
30	10.5 ± 2	14.0 ± 1	19.4 ± 2	108 ± 25

*Phase 1 default conditions were used for all determinations. In particular, $V^\#$ and $A^\#$ are both equal to one.
‡An R_{CD} value of ∞ implies that no transition to Class D could be detected for rending numbers of up to 10^3.

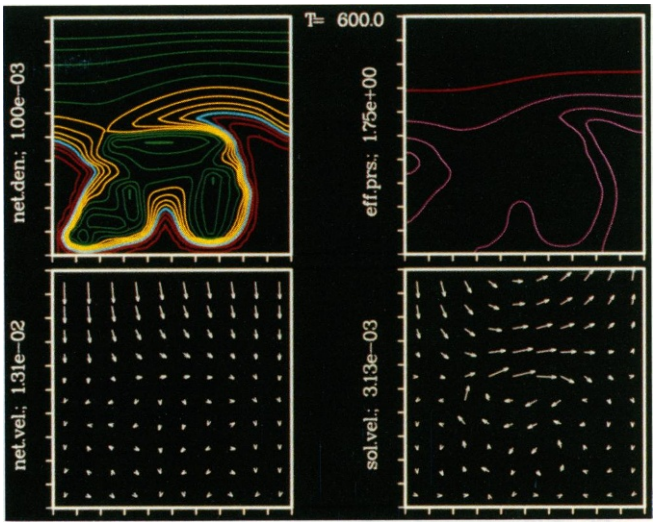

FIGURE 8 The reservoir boundary condition. Parameters in this computation are matched with D_4 (Fig. 7 *B*) except that the reservoir method is used for the top boundary condition instead of the hard wall method. Notice the change in the solution velocity field.

Variations of the network viscosity ratio ($V^\# = \Lambda_n/M_n$) between 0 and 10 can shift the subtype of class D computations and cause other minor variations similar to the effects of perturbing the initial conditions. Aside from such small effects, it seems that for the most part the behavior of the reactive flow model depends only on an effective or lumped network viscosity, $2M_n + \Lambda_n$.[4]

Fig. 8 shows a computation that is exactly matched with the computation shown in Fig. 7 *B*, except that it uses the reservoir method to describe the top boundary condition. By comparing Figs. 8 and 7 *B*, it can be seen that there is very little change in the general motion and distribution of the network phase. The magnitude of these changes is similar to the magnitude of change caused by variation of the initial conditions. In contrast, comparison of the solution velocity fields for Figs. 8 and 7 *B* shows that in the hard-wall method an eddy or vortex of solution is trapped against the upper boundary, whereas in the reservoir method this vortex does not exist since mass in the solution phase can freely leave the reaction vessel through the top boundary. Except for such minor but interesting effects, we have found no cases where the treatment of the top boundary is important.

In cytoplasmic flaring, it is observed that endoplasmic material erupts from the surface of the cytoplasmic mass. Concerning such eruptions, it is important to know the source of the fluid. A distant source of fluid implies that this is a tendency for solution phase material to percolate deep into the interior of the cytoplasmic mass. Such deep

[4]A similar result was obtained previously in our study of unreactive network (Dembo et al., 1986). However, in that case there was a slightly different definition of effective viscosity.

percolation could allow contraction of network at one point on the perimeter of the cytoplasmic mass to drive an eruption of endoplasm at a distant point. Furthermore, this sort of phenomenon would contradict our assumption of zero flux at the bottom of the reaction vessel. To investigate the possibility of deep percolation, we carried out controls in which a large hydraulic permeability of the lower boundary of the reaction vessel was assumed. In such computations there is some percolation of fluid through the lower boundary. But for realistic values of the permeability, the velocities of flow are negligible. This is because the pressure head caused by contraction at the base of an ectoplasmic protrusion has many opportunities to be dissipated locally. In particular, there is less resistance if solution flows outward or laterally rather than down into the interior.

Fig. 9 illustrates the effects caused in a class D computation if the width of reaction vessel is increased while the height remains unchanged. All parameters for the computation shown in Fig. 9 are the same as in D_2 (Fig. 7 *B*) except that the value of L_x is doubled. In many such matched computations we find that if the width of the reaction vessel is increased (i.e., if $A^{\#} > 1$), then in the final steady state there is little effect on the dynamical mode or on spatially averaged quantitative features of the motion (compare Fig. 9 with Fig. 7 *B*).

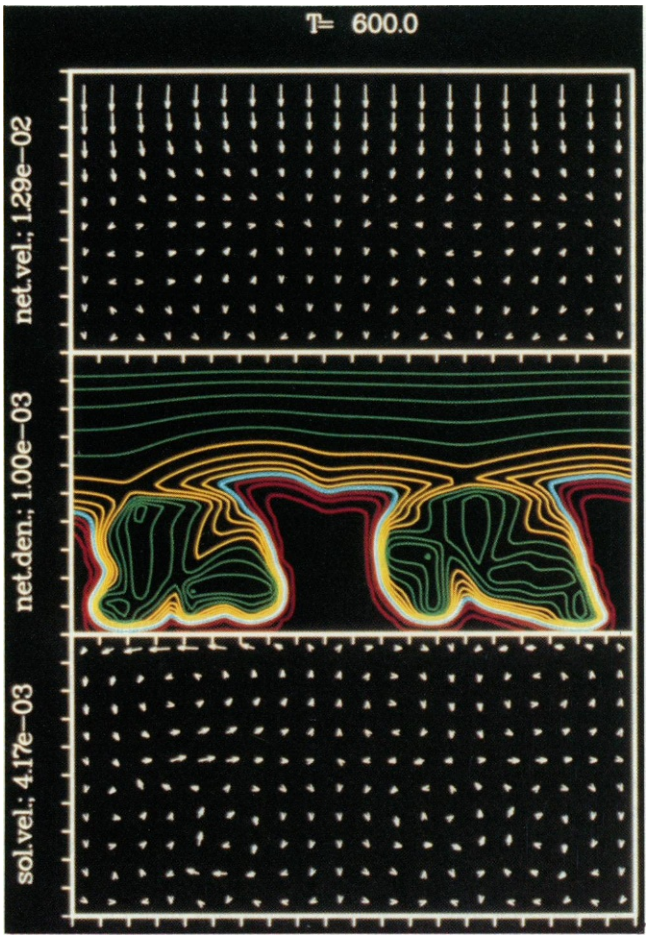

FIGURE 9 The aspect ratio of the reaction vessel. Parameters in this computation are matched with D_4 (Fig. 7 *B*) except that the aspect ratio of reaction vessel is doubled. As shown, use of a wide reaction vessel simply leads to quasi-periodic repetition of the tableau found in a square vessel.

We conclude that a wide reaction vessel simply leads to a quasi-periodic repetition or piecing together of tableau that are similar in structure and size to the patterns seen in a square reaction vessel. The natural spacing between protrusions is always about twice the height of an individual protrusion. The natural spacing is independent of the initial conditions. We conclude that the use of mirror symmetry boundary conditions on the left and right walls of the reaction vessel and the use of square reaction vessel does not preclude an analysis of laterally extended physical systems.

DISCUSSION

A necessary feature of any successful mechanical model of the cytoplasm is the existence of states of continuous automatic motion. The computations we have reported here demonstrate that the reactive flow model satisfies this fundamental requirement. For states of automatic motion to occur in the reactive flow model, an appropriate form of the chemical reaction of network assembly and breakdown is an absolutely indispensable ingredient. The form of the terms describing the chemical reaction in the reactive flow model [i.e., the term $(\hat{\theta}_n - \theta_n)/T_{eq}$ in Eq. A3] is such that chemical reaction tends to produce a distribution of contractile network that has high entropy (i.e., a uniform distribution). Mechanical factors tend to produce a distribution of low entropy (i.e., a clumped or contracted distribution). Generalized models that retain the spirit of the dialectic between mechanics and chemistry envisioned by the reactive flow model will also predict continuous automatic motion.

In many of the computations we have described there exists a sharp dichotomy between regions of low and high network density. After some attempts, we have found it very difficult to understand or discuss the predictions of the reactive flow model without introducing terminology (i.e., the terms "endoplasm" and "ectoplasm") for denoting this dichotomy. (We could have just as well used the terms "sol" and "gel," but these have undesirable rheological connotations.) The endoplasm–ectoplasm dichotomy derives from the form of the constitutive law governing the combined stress produced by solvation and contraction, i.e., the term $\psi_F[\theta_n + \sigma(\theta_n + \ell n\ \theta_s)]$ that appears in Eq. A5. The essential factor is that as the network density increases, there is a point at which the stress driving contraction vanishes. A large class of models that include this properly will also give rise to an endoplasm–ectoplasm dichotomy.

For many years cell biologists have recognized that something resembling what we call the endoplasm–

ectoplasm dichotomy exists in the cytoplasm of amoeboid cells. Furthermore, parameters such as "the percentage of gel" have long been measured and have been found to have important correlations with physiological activity (see Allen, 1961, for a discussion of these data). In light of these facts, we presently regard the predicted existence of endoplasm and ectoplasm to be a successful and desirable aspect of the reactive flow model. We know of no other model that offers a quantitative formulation of the free boundary problem of endoplasm and ectoplasm nor one that offers the practical possibility of computing the behavior of these two elements. Nevertheless, it must be remembered that this whole house of cards rests on a question of interpretation of remote observations. It is necessary to obtain better evidence that the regions of high network density predicted by the reactive flow model are actually equivalent in all relevant details to the ectoplasmic regions of real cells.

Our analysis of the reactive flow model has brought to light the importance of dynamical modes and of the interconversions of dynamical modes. The results of Taylor et al. and of Kuroda establish that the mechanical activity of dissociated cytoplasm also falls naturally into various modes. Interconversions between modes were shown to occur as a result of depletion of the physiological medium or as a result of specific alterations in the medium.

Of the various modes of motility predicted by the reactive flow model, the chaotic, or E mode, has the greatest degree of experimental support. An example of such support is Kuroda's observation of a regime consisting of scattered contractile centers; other examples are discussed in the section on experimental background. Recently it has even been possible to obtain chaotic modes in reconstituted cytoplasm consisting of specified amounts of purified actin, myosin, and other well-characterized reagents (Higashi-Fujime, 1982).

The prevalence of type E behavior under in vitro conditions is a predictable and natural consequence of the phase structure of parameter space (see Table III). A system that has enough contractility to give rapid motion will satisfy the condition $C^{\#}(1 - D^{\#})^2 \gtrsim 1$, and any system that has a sufficiently large volume will have a rending number greater than R_{DE}. To obtain the other modes predicted by the reactive flow model, physiological conditions and system size must be controlled within specified tolerances.

In terms of the various dynamical modes of the reactive flow model, one naturally identifies the cytoplasmic flares reported by Taylor et al. as a case of the fortification subtype of the D mode. Some of the simulations we have presented of the fortification mode (particularly D_5) have many of the basic features described by Taylor et al.: material flows outward from the surface of the cytoplasmic mass for a considerable distance, makes a loop, and returns. Near the point of turning there is an endoplasm-to-ectoplasm transition. The relative rate of outward endoplasm flow is much faster than the speed of downward flow within the protrusion. The speed of return flow is highly variable and can even be zero if the rending number is such that the ectoplasmic protrusion is close to pinching off from the main cytoplasmic mass. We have even arranged the choice of physical parameters (see Table IV) so that the actual size and spacing of the ectoplasmic protrusions and the actual flow velocities in computations D_3–D_6 are in rough agreement with the observations of Taylor et al.

Although the reactive flow model can reproduce much of the detail observed in the flaring reaction, other aspects of the simulations are not so satisfactory. Even in the best cases, the flares that one obtains numerically are too thick, especially at the base; and they lack the kind of long, graceful loops and bends described by Taylor et al. Furthermore, the ratio of inter-flare spacing to flare height is too large by at least a factor of two. Part or all of these difficulties could arise from the fact that the numerical simulations are two-dimensional (i.e., numerical flares are flat, whereas real flares are cylindrical).

A related source of error could arise because the simulations neglect the effects of adhesion between the cytoplasm and the glass slide and/or coverslip. Other factors that could contribute to the deficiencies in our calculations are discussed in detail elsewhere (see Appendix I of Dembo and Harlow, 1986).

Consistency with the reactive flow model requires that the rosettes observed by Kuroda be interpreted as a case of type D behavior. However, it is not clear whether the phenomena should be regarded as an example of the crypt subtype or of the fortification subtype (see discussion of Figs. 5 and 7 *D*). In either event, the basic configuration of a large ectoplasmic mass surrounded by a close packed array of vigorous convection cells can be obtained. For both fortification and crypt solutions, the model predicts that each convection cell is associated with a small bump or bleb on the surface of the ectoplasm. Close examination of Fig. 1 *B* reveals the presence of bumps of the sort expected.

In addition to an account of the existing observations, the reactive flow model makes several predictions about the systems of Taylor et al. and Kuroda that offer the possibility of additional tests. The model predicts that for certain conditions the system of Taylor et al. will give rise to states of E type behavior analogous to the contractile centers reported by Kuroda. The model also predicts the existence of C-type modes for both systems. According to the model, a simple way to induce E-type behavior would be to proportionally enlarge the volumes of the cytoplasmic mass and the physiological solution. C-type behavior could be induced by scaling down the volumes. Finally, for special conditions the model predicts the occurrence of endoplasmic crypts within the cytoplasmic mass for either system.

In formulating models of cytoplasmic mechanics (e.g., the frontal contraction model or the ectoplasm contraction model), there is a tendency to focus excessively on the site or locus of contractile activity. This implicitly leads to

violations of the principal of material objectivity. In the case of contractile networks, material objectivity requires that the various filaments of the network can have no a priori knowledge of their position in space. Each infinitesimal element of the network must act as an independent automaton on the basis of purely local information. In particular, all elements of a network, no matter where they are in space, must obey the same constitutive law for development of contractile stress.

A license to violate material objectivity is frequently justified by proposing that gradients of concentration of calcium ion or some other diffusible factor can play the part of *Deus ex machina*. This is really a variation on the old hypothesis of "morphogens" in developmental biology. There is no doubt that calcium ion and other diffusible substances can greatly influence the important rheological and chemical parameters of contractile networks, but this does not justify a morphogen model. The critical question concerns the encoding of information. One must thus ask whether functional gradients of morphogen occur for more than a short time, or whether diffusion plus the mixing action of the cytoplasmic motion itself is enough to rapidly destroy any such gradients. In the case of Ca^{++} control of contractility, this means that one must distinguish between (*a*) models in which Ca^{++} causes a long-term but spatially global increase in contracivity, (*b*) models in which Ca^{++} cause a spatially localized change in contractility that rapidly dissipates, and (*c*) a true morphogen model in which Ca^{++} causes spatially localized variations in contractility that remain stable for long times.

There is nothing contradictory about the idea of morphogens and the idea of the reactive flow model (see Appendix I of Dembo and Harlow, 1986). Nevertheless, the present study indicates that the observed phenomenon in dissociated cytoplasm can be understood, at least to some extent, without involving a morphogen-like substance. It remains to be seen if this is also true of intact cells.

APPENDIX A

Summary of Equations

In this appendix we summarize the various dynamical equations that constitute the Reactive Flow Model of contractile networks. In the interior of the reaction vessel the equations are: the excluded volume relation

$$\theta_n + \theta_s = 1; \tag{A1}$$

the mass conservation equations

$$0 = \nabla \cdot (\theta_s \Omega_s) + \nabla \cdot (\theta_n \Omega_n) \tag{A2}$$

and

$$\delta_t \theta_n = -\nabla \cdot (\theta_n \Omega_n) + (\tilde{\theta}_n - \theta_n) / T_{eq}; \tag{A3}$$

the momentum conservation equations

$$0 = \nabla(\Lambda_s \theta_s \nabla \cdot \Omega_s) + 2(\nabla \cdot \mathrm{M}_s \theta_s \nabla)\Omega_s + \nabla \times (\mathrm{M}_s \theta_s \nabla \times \Omega_s) + \phi \theta_s \theta_n (\Omega_n - \Omega_s) - \theta_s \nabla P_F \tag{A4}$$

and

$$0 = \nabla(\Lambda_n \theta_n \nabla \cdot \Omega_n) + 2(\nabla \cdot \mathrm{M}_n \theta_n \nabla)\Omega_n + \nabla \times (\mathrm{M}_n \theta_n \nabla \times \Omega_n) + \phi \theta_s \theta_n (\Omega_s - \Omega_n) - \theta_n \nabla \mathrm{P}_F + \nabla\{\psi_F[\theta_n + \sigma(\theta_n + \ell \mathrm{n}\, \theta_s)]\}. \tag{A5}$$

If $\mathbf{R}_b$ is a location on the boundary of the reaction vessel, then the relevant characteristics of the reaction vessel at $\mathbf{R}_b$ are specified by five functions:

$SLP_s(\mathbf{R}_b)$ = +1 if the boundary is free-slip with respect to solution
= −1 if the boundary is no-slip with respect to solution.
$SLP_n(\mathbf{R}_b)$ = +1 if the boundary is free-slip with respect to network
= −1 if the boundary is no-slip with respect to network.
$STK(\mathbf{R}_b)$ = +1 if the boundary is sticky with respect to network
= −1 if the boundary is no-stick with respect to network.
$H_C(\mathbf{R}_b)$ = hydraulic conductivity of boundary.
$P_{ex}(\mathbf{R}_b)$ = effective external pressure on the boundary.

In terms of these descriptive functions, we obtain the tangent boundary conditions on solutions and network velocity fields:

$$(1 + SLP_s)(\mathbf{n} \cdot \nabla)(\Omega_s \cdot \tau) + (1 - SLP_s)(\Omega_s \cdot \tau) = 0 \tag{A6}$$

$$(1 + SLP_n)(\mathbf{n} \cdot \nabla)(\Omega_n \cdot \tau) + (1 - SLP_n)(\Omega_n \cdot \tau) = 0; \tag{A7}$$

the normal boundary conditons on the solution and network velocity fields

$$\mathbf{n} \cdot \Omega_s = H_c(P_F - P_{ex}) \tag{A8}$$

and

$$0 = (1 + STK)(\mathbf{n} \cdot \Omega_n) + (1 - STK)(\Lambda_n \nabla \cdot \Omega_n + 2M_n(\mathbf{n} \cdot \nabla)(\mathbf{n} \cdot \Omega_n) + \Psi_F); \tag{A9}$$

and finally, the boundary condition on the network density

$$(1 + STK)(\mathbf{n} \cdot \nabla\theta_n) + (1 - STK)\theta_n = 0 \tag{A10}$$

APPENDIX B

In this appendix we wish to show that if there is a strong endoplasmectoplasm differentiation and if the network phase is everywhere dilute, then at long times the fraction of the reaction vessel occupied by ectoplasm will be approximately equal to the density ratio, D^{θ}.

By hypothesis, the reaction vessel can be divided into subregions of endoplasm and ectoplasm. Furthermore, if the volumes of these subregions are V_{ecto} and V_{endo}, respectively, then

$$V_{ecto} + V_{endo} \sim V_{total}. \tag{B1}$$

The total amount of network contained in the reaction vessel is

$$\int_{V_{total}} \theta_n(\mathbf{r})d\mathbf{r} \sim \int_{V_{endo}} \theta_n(\mathbf{r})d\mathbf{r} + \int_{V_{ecto}} \theta_n(\mathbf{r})d\mathbf{r}. \tag{B2}$$

By definition, the density of network in endoplasmic regions is very low; whereas the density in ectoplasmic regions is approximately equal to $\hat{\theta}_n$. Therefore we conclude from Eq. B2 that

$$\int_{V_{Total}} \theta_n(\mathbf{r})d\mathbf{r} \sim \hat{\theta}_n V_{ecto} \sim 2V_{ecto}/\sigma, \tag{B3}$$

where we have used the fact that $\hat{\theta}_n \sim 2/\sigma$ in the dilute network limit.

If we now integrate the equation of network mass conservation (see Appendix A) over the entire reaction vessel, we obtain

$$\frac{\partial}{\partial t}\int_{V_{\text{Total}}}\theta_n d\mathbf{r} = \int_{V_{\text{Total}}}\nabla\cdot(\theta_n\Omega_n)d\mathbf{r} + \frac{1}{T_{eq}}\int_{V_{\text{Total}}}(\tilde{\theta}_n-\theta_n)d\mathbf{r}. \quad \text{(B4)}$$

The first integral to the right vanishes due to the boundary conditions. We thus conclude that

$$\frac{d}{dt}\int_{V_{\text{Total}}}\theta_n d\mathbf{r} = \frac{1}{T_{eq}}\tilde{\theta}_n V_{\text{Total}} - \frac{1}{T_{eq}}\int_{V_{\text{Total}}}\theta_n d\mathbf{r}. \quad \text{(B5)}$$

This expression makes clear that at long times

$$\int_{V_{\text{Total}}}\theta_n d\mathbf{r} \sim \tilde{\theta}_n V_{\text{Total}}. \quad \text{(B6)}$$

At this point, substitution from Eq. B6 into Eq. B3 directly yields the desired result:

$$\frac{V_{\text{ecto}}}{V_{\text{Total}}} \sim \tilde{\theta}_n/\hat{\theta}_n \sim \tilde{\theta}_n\sigma/2 \equiv D'. \quad \text{(B7)}$$

This work was supported by grants K04-AI00966-01 and R01-AI21002-01 from the National Institutes of Health. Work was also supported by the United States Department of Energy.

Received for publication 28 April 1986 and in final form 26 August 1986.

REFERENCES

Allen, R. D., J. W. Cooper, and P. J. Hall. 1960. Streaming in cytoplasm dissociated from the giant amoeba, *Chaos-chaos*. *Nature (Lond.)*. 187:896–899.

Allen, R. D. 1961. A new theory of amoeboid movement and protoplasmic streaming. *Exp. Cell Res.* 8(Suppl.):17–31.

Dembo, M., and F. Harlow. 1986. Cell motion, contractile networks, and the physics of interpenetrating reactive flows. *Biophys. J.* 50:109–121.

Dembo, M., M. Maltrud, and F. Harlow. 1986. Numerical studies of unreactive contractile networks. *Biophys. J.* 50:123–137.

Feigenbaum, M. J. 1980. Universal behavior in nonlinear systems. *Los Alamos Science*. 1:4–28.

Higashi-Fujime, S. 1982. Active movement of bundles of actin and myosin filaments from muscle: A simple model of cell motility. *Cold Spring Harbor Symp. Quant. Biol.* 46:69–75.

Kuroda, K. 1979. Movement of cytoplasm in a membrance-free system. *In* Cell Motility: Molecules and Organization. S. Hatano, H. Ishikawa, and H. Sato, editors. University Park Press, Baltimore. 347–362.

Pollard, T., and S. Ito. 1970. Cytoplasmic filaments of amoeba *Proteus*. I. The role of filaments in concistency changes and movement. *J. Cell Biol.* 46:267–289.

Taylor, D. L., J. S. Condeelis, P. L. Moore, and R. D. Allen. 1973. The contractile basis of amoeboid movement. I. The chemical control of motility in isolated cytoplasm. *J. Cell Biol.*59:378–394.

Thompson, C. M., and L. Wolpert. 1963. Isolation of motile cytoplasm from amoeba *Proteus*. *Exp. Cell Res.*32:156–160.